

Quantum Error-Correction-Enhanced Magnetometer Overcoming the Limit Imposed by Relaxation

David A. Herrera-Martí,¹ Tuvia Gefen,¹ Dorit Aharonov,² Nadav Katz,¹ and Alex Retzker¹
¹*Racah Institute of Physics, The Hebrew University of Jerusalem, Jerusalem 91904, Givat Ram, Israel*
²*School of Computer Science and Engineering, The Hebrew University, Jerusalem 91904, Israel*
 (Received 30 September 2014; revised manuscript received 10 June 2015; published 9 November 2015)

When incorporated in quantum sensing protocols, quantum error correction can be used to correct for high frequency noise, as the correction procedure does not depend on the actual shape of the noise spectrum. As such, it provides a powerful way to complement usual refocusing techniques. Relaxation imposes a fundamental limit on the sensitivity of state of the art quantum sensors which cannot be overcome by dynamical decoupling. The only way to overcome this is to utilize quantum error correcting codes. We present a superconducting magnetometry design that incorporates approximate quantum error correction, in which the signal is generated by a two qubit Hamiltonian term. This two-qubit term is provided by the dynamics of a tunable coupler between two transmon qubits. For fast enough correction, it is possible to lengthen the coherence time of the device beyond the relaxation limit.

DOI: 10.1103/PhysRevLett.115.200501

PACS numbers: 03.67.Pp, 06.20.-f, 85.25.Hv

Introduction.—Quantum technologies have attracted great attention over the last decade due to the outstanding enhancements derived from the ability to manipulate physical systems to the limit dictated by quantum mechanics. Common to all of these technologies is the necessity to decouple quantum systems from their environment, while maximizing control. In the context of quantum metrology, a single highly coherent probe can be used to measure very weak magnetic fields via Ramsey interferometry, with a sensitivity that scales as $\delta B \propto 1/\sqrt{TT_2}$ [1,2], where T is the total experiment time and T_2 is the probe coherence time. Whereas pure dephasing noise can be accounted for by means of refocusing techniques [3–12], the relaxation-limited coherence time, i.e., $T_2 = 2T_1$, is a fundamental limit to sensing. In this Letter, we propose an experimental setup based on superconducting devices in which T_1 can be prolonged while sensing a weak signal.

Quantum-error-correcting codes (QECCs) and sensing.—Quantum codes were originally devised to lengthen coherence times of quantum registers [13–16], and it was realized that if the noise rate is below a threshold constant, quantum coherence can be maintained for arbitrarily long times [17–19]. Recently it was observed that introducing QECCs will increase the sensitivity in different scenarios [20–23], which is extremely promising for future theoretical and experimental developments. QECCs can be designed to distinguish the error from the signal by probing a specific n -qubit interaction, which limits the use of QECCs to sense exotic interactions. However, obtaining n -qubit Hamiltonian terms out of single body interactions by means of virtual transitions offers no advantage, as the increase in lifetime resulting from error correction is cancelled by a decrease in strength of the effective signal [22].

The smallest operator that exact QECCs can probe is a three body interaction [14,15], since these codes correct all single-qubit quantum errors. In order to overcome this restriction, we resort to approximated QECCs [24], where relaxation errors can be corrected while probing two-qubit interactions, such as the one offered by a flux-dependent tunable coupler. This code is defined by the codewords $|\bar{0}\rangle = |\psi^+\rangle_{1,2}|\psi^+\rangle_{3,4}$ and $|\bar{1}\rangle = |\psi^-\rangle_{1,2}|\psi^-\rangle_{3,4}$, where $|\psi^\pm\rangle = (1/\sqrt{2})(|00\rangle \pm |11\rangle)$. This code is stabilized [16] by $S_4 = \{S_1 = \sigma_1^X \sigma_2^X \sigma_3^X \sigma_4^X, S_2 = \sigma_1^Z \sigma_2^Z I_3 I_4, S_3 = I_1 I_2 \sigma_3^Z \sigma_4^Z\}$ and its logical operators are $\bar{X} = \sigma_1^Z I_2 \sigma_3^Z I_4$ and $\bar{Z} = \sigma_1^X \sigma_2^X I_3 I_4$.

We assume that refocusing techniques and qubit design [25–37] can be used to push the system’s coherence to the relaxation limit. In this scenario, the signal is measured by performing a Ramsey-type experiment at the logical level [20,23]. Whereas the physical qubits decay at any time, performing correction after short enough lapses of duration τ_{EC} will reduce the failure probability at the logical level.

Tunable coupler.—The fundamental problem behind QECC-enhanced quantum sensing is the engineering of a many-body Hamiltonian term with strength proportional to the signal to be estimated. We now explain how to obtain a two-body Hamiltonian term using a tunable coupler between two off-resonant transmon qubits [32,33]. The coupler’s Hamiltonian is $H = g_s \sigma_1^Z \sigma_3^Z + g'_s (\sigma_1^+ \sigma_3^- + \sigma_1^- \sigma_3^+)$, where the strength of the coupling energies g_s and g'_s have been calculated to be of order 1 and 10 MHz, respectively [32]. A flux threading through the tunable coupler can be used to bias it at the optimal response point, i.e., $\Phi_{\text{coupler}} = \Phi_{\text{signal}} + \Phi_{\text{bias}}$. For very weak signals compared to the flux quantum, i.e., for $\Phi_{\text{signal}}/\Phi_0 \ll 1$, the response to a threading signal flux can be linearized.

As can be seen from rewriting $\sigma_1^+ \sigma_3^- + \text{H.c.} = \frac{1}{2}(\sigma_1^X \sigma_3^X + \sigma_1^Y \sigma_3^Y) = (\sigma_1^X \sigma_3^X / 2)(I - \sigma_1^Z \sigma_3^Z)$, the effect of the flip-flop term induces uncorrectable evolution outside of the code space. To cancel this effect, qubits at both ends of the tunable coupler must be far-detuned so that the energy transfer between them is suppressed. Incidentally, the reason why a simple SQUID junction cannot be used in order to generate a logical signal is that in the computational basis, the SQUID Hamiltonian is as a flip-flop term, which nevertheless does not preclude other interesting applications [38]. For a detuning Δ between qubits 1 and 3, it is then possible to rewrite the tunable coupler interaction as

$$H_{\text{signal}} = g_s \sigma_1^Z \sigma_3^Z + \mathcal{O}(g_s^2 / \Delta), \quad (1)$$

up to a known correction [39] at the logical level, due to the flip-flop interaction, which is negligible for large detunings.

Noise and error correction.—The setting presented in Fig. 1 bears many similarities with the layout of Ref. [35], where extremely fast quantum gates with high fidelity have been demonstrated. In particular, it was found that the lifetimes are limited by decoherence in the devices and not by noise in gates or in the read-out lines. We therefore model each correction operation as a perfect gate followed by single- and two-qubit depolarizing noise with per-gate error probability p_{gate} .

Relaxation at a rate γ can be generalized to multiple qubits by $\mathcal{R}(\rho) = \sum_{s \in \{0,1\}^4} K_s \rho K_s^\dagger$ with $K_s = K_{s_1} K_{s_2} K_{s_3} K_{s_4}$, where $K_1 = \sqrt{\gamma \tau_{\text{EC}}} \sigma^-$ describes a decay event, and $K_0 = |0\rangle\langle 0| + \sqrt{1 - \gamma \tau_{\text{EC}}} |1\rangle\langle 1|$ reflects the fact that if no decay occurred, the probability of finding the qubit in the excited state has decreased. There are only five Kraus operators that act on the state to first order, $K_{0000}, K_{0001}, \dots, K_{1000}$.

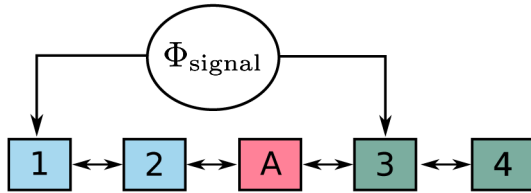


FIG. 1 (color online). Diagrammatic layout of the QECC-enhanced magnetometer. Each superconducting trasmon qubit is represented by a numbered box, and its nearest neighbor tunable coupling (cf. Refs. [32,35,37]) is represented by a two-headed arrow. Between qubits 1 and 3, a tunable coupler with a flux-dependent strength $g_s(\Phi_{\text{signal}})$ is interrupted by an inductive loop (cf. Ref. [39]). This signal is obtained by placing the sensor in proximity to the sample to be measured. Our sensing protocol relies on our ability to prepare the initial state $|\Psi_0\rangle = |\bar{0}\rangle = |\psi^+\rangle |\psi^+\rangle$, which is left to precess according to $H_{\text{signal}} = g_s \sigma_1^Z \sigma_3^Z$. Then, by measuring frequency of the oscillations one is able to infer the value of the magnetic flux threading the coupler.

It was shown in Ref. [24] that it is possible to outperform standard QECC by relaxing the conditions for error correction. If instead of demanding exact correction for a given error channel, we demand that the approximate QECC retrieves the correct state up to first order in the error probability, then small codes exist that can approximately correct for errors [39]. Our error correction protocol \mathcal{C} , subsumed in Fig. 2, ensures that the fidelity of the corrected state is one up to second order, $\mathcal{F} = \text{tr}(\mathcal{C} \circ \mathcal{R}(\rho) \rho) \geq 1 - \mathcal{O}((\gamma \tau_{\text{EC}})^2)$, even if the code is not exact. Depending on the outcome of the parity measurement [Fig. 2(a)], one of the five possible approximate correction operations is applied [Fig. 2(b) and its permutations, and Fig. 2(c)]. Each of these corrections can be done using single- and two-qubit gates and restores the original state to second order [39]. Each SWAP gate, needed to perform non-nearest neighbour gates, adds an overhead equivalent to three CONTROLLED-PHASE gates (of duration 40 ns each [35]), and measurements are assumed to take 200 ns [40],

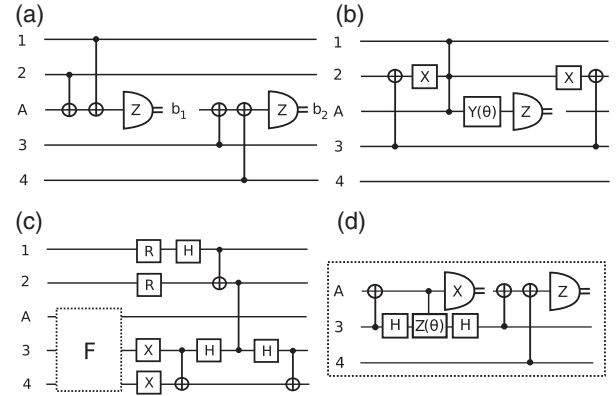


FIG. 2. Error correction procedure. (a) To detect which of the five first-order operators occurred, a pairwise parity check in the four qubits is stored in two bits (b_1, b_2). (b) If $(b_1, b_2) = (0, 0)$, the state is projected in $K_{0000}^\dagger \rho K_{0000}$ and this circuit partially undoes the error rotating by $\theta = \tan^{-1}((1 - \gamma \tau_{\text{EC}})^2)$ in the space of $\{|0000\rangle, |1111\rangle\}$. The ancilla, A, is initially prepared in the $|+\rangle$ state and $Y(\theta)$ represents a rotation of θ around the Y axis. The CONTROLLED-CONTROLLED-PHASE (CCPhase) gate can be decomposed in a series of five two-qubit gates. This approximately corrects the error, up to a known Pauli operator that will depend on the measurement outcome. (c) If $(b_1, b_2) = (1, 0)$, then the state is projected in a mixture of $A_{1000}^\dagger \rho A_{1000}$ and $A_{0100}^\dagger \rho A_{0100}$. A filter is applied in order to regain the relative amplitude between the decayed codewords, followed by a resetting (R) of the first two qubits. Qubits 3 and 4 undergo a $X_3 X_4$ operation to restore the correct coherence and the following gates are meant to reconstruct the codewords. An equivalent procedure holds for $(b_1, b_2) = (0, 1)$. For $(b_1, b_2) = (1, 1)$, which happens only to second order, no correction is possible and the state is left untouched. (d) Filter. The ancilla is initialized in the $|1\rangle$ state and a conditioned rotation around the Z axis of $\phi = \cos^{-1}(1 - \gamma \tau_{\text{EC}})$ is carried out to transfer part of the amplitude of the $|00\rangle$ state into the odd parity subspace. If even parity is detected, then the correction continues, and it aborts otherwise.

rendering the correction doable in about $2 \mu\text{s}$, with less than thirty two-qubit and a few tens of single-qubit gates on average. This is entirely feasible with current technology [36].

Below the threshold value depicted in Fig. 3(a), the error probability at the logical level, $p_{\text{logical}} = 1 - \mathcal{F}$, decreases quadratically as the physical probability $p = 1 - \exp(-\gamma\tau_{\text{EC}}) \approx \gamma\tau_{\text{EC}}$ is reduced since physical errors occurring at first order are corrected. Importantly, trying to correct for relaxation will introduce errors due to imperfect gates, ancilla preparation, and measurements. These errors cannot be accounted for, as a consequence of the four qubit code being too small, and will unavoidably result in a decrease of fidelity. However, larger codes could in

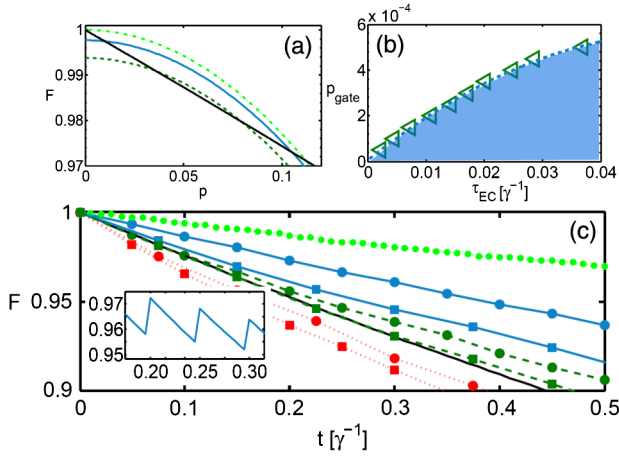


FIG. 3 (color online). (a) The fidelity of the initial state $|\bar{0}\rangle$ after undergoing relaxation with probability p . The solid black line represents the decay of an unencoded probe initially in the superposition state $|+\rangle$. QECC undoes errors to first order in the relaxation probability, as reflected by a quadratic curve (light green, dashed line) in which linear terms do not contribute to fidelity loss. The solid blue line and the dark green dashed line represent the loss of fidelity when the gates in the error correction procedure introduce error with $p_{\text{gate}} = 10^{-2}\%$ and $p_{\text{gate}} = 5 \times 10^{-2}\%$, respectively. (b) Errors introduced in the correction procedure cause a fidelity loss, at a rate depending on the time lapse τ_{EC} . The shaded area below the curve is the area in which there is a sensitivity increase over the unencoded case. (c) Decay of the fidelity for a probe initially prepared in the state $|\bar{+}\rangle$, for three different frequencies of error correction, averaged over 10^4 runs. Again, the solid black line denotes the evolution of an unencoded probe. The top, light green curve corresponds to $\tau_{\text{EC}} = 0.01\gamma^{-1}$ and a gate error of $p_{\text{gate}} = 5 \times 10^{-3}\%$. The filled circles (squares) denote error correction is carried out every $\tau_{\text{EC}} = 0.05\gamma^{-1}$ ($0.075\gamma^{-1}$). The blue solid lines (dashed green) correspond to $p_{\text{gate}} = 10^{-2}\%$ ($5 \times 10^{-2}\%$), showing that there is indeed a benefit for high enough gate fidelities and frequencies. The red dotted lines correspond to $p_{\text{gate}} = 0.1\%$, showing that applying error correction is actually worse than using the unencoded probe. (inset) Fine-grained evolution for $p_{\text{gate}} = 5 \times 10^{-2}\%$ and $\tau_{\text{EC}} = 0.05\gamma^{-1}$. Between two rounds of error correction, the fidelity decays exponentially.

principle be used to correct for these errors. In our case, it is still possible to achieve an improvement, provided that the fidelity of the gates is above a threshold that will depend on the time lapse τ_{EC} . As depicted in Fig. 3(c), our simulations confirm that lengthening the lifetime beyond the relaxation limit is indeed possible for frequent corrections and sufficiently good gates. In Fig. 4 the time evolution of the probe in two scenarios is shown. When the signal is strong compared to the decay rate, it becomes apparent that the contrast can be maintained for times greatly exceeding the relaxation limit. For signals weaker than the inverse lifetime an encoded probe can feel the signal for a time proportional to the inverse effective lifetime, whereas in the unencoded case the signal is rapidly obliterated by the decay.

Sensitivity analysis.—The sensitivity of our setup is given by $\delta B = \delta P / |dP/dB|$, where P is the average value of the measured operator, and the optimal precision scaling can be analytically calculated to be

$$\delta B = \frac{1}{|dg_s/dB|} \sqrt{2e\Gamma^{\text{eff}}/T}, \quad (2)$$

where Γ^{eff} is the effective noise rate at the logical level, which is estimated analytically [39] to be $\Gamma^{\text{eff}} \leq 4\gamma^2\tau_{\text{EC}} + \xi p_{\text{gate}}/\tau_{\text{EC}}$ in the absence of pure dephasing. The parameter

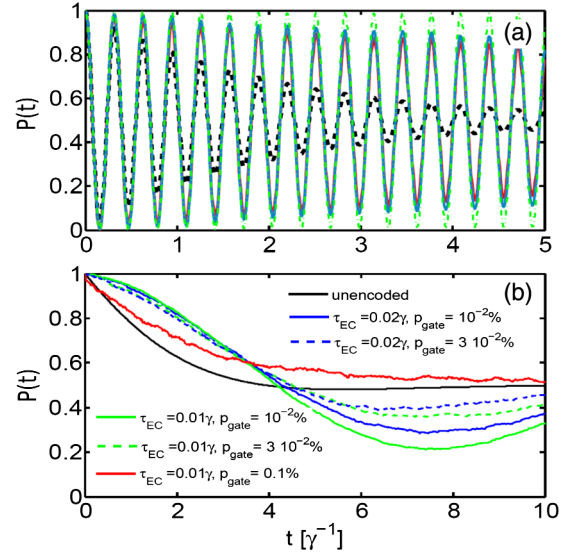


FIG. 4 (color online). Simulation (averaged over 500 runs) of the population evolution $P(t) = \text{tr}(|\Psi_0\rangle\langle\Psi_0|\rho(t))$ in the presence of a signal. (a) The signal strength is larger than the decay rate, $g_s = 10\gamma$. The black dashed line shows the evolution of the unencoded probe. The red, blue, and dashed green lines represent the evolution with $p_{\text{gate}} = 10^{-2}\%$, $\tau_{\text{EC}} = 10^{-2}\gamma^{-1}$; $p_{\text{gate}} = 5 \times 10^{-3}$, $\tau_{\text{EC}} = 5 \times 10^{-3}$; and $p_{\text{gate}} = 0$, $\tau_{\text{EC}} = 10^{-3}$, respectively. This shows that the fringes contrast can be maintained well beyond the relaxation limit. (b) The signal strength is smaller than the decay rate, $g_s = \gamma/5$. Whereas small signals cannot be resolved by a decaying probe, using error correction ensures that the probe remains sensitive to weak signals.

ξ is a numerically obtained prefactor which encapsulates the collective error of all the gates in the correction protocol [39].

Since $|dg_s/dB| = |dg_s/d\Phi_{\text{signal}}d\Phi_{\text{signal}}/dB| = |dg_s/d\Phi_{\text{signal}}A_{\text{coupler}}|$, the larger the area of the coupler, the smaller the magnetic fields that can be measured, at the expense of reducing the spatial resolution of the device. For a linearized response reported in Ref. [32], a coupler area size of roughly $100 \mu\text{m}^2$, $T_2 \approx 40 \mu\text{s}$ [37], and in the absence of error correction, the sensitivity of our design is estimated to be upper-bounded by $\sim 500 \text{ pTHz}^{1/2}$. It is within reach to improve the circuit parameters to increase the sensitivities by more than 1 order of magnitude. This sensitivity compares with those of modern SQUID magnetometers, lying in the $\text{nTHz}^{1/2}$ [41] and $\text{fTHz}^{1/2}$ [42] range, depending on application and bandwidth. The magnetometer reported in Ref. [43] operates in the Josephson dispersive regime and its sensitivity, not limited by thermal fluctuations, is estimated to fall in the $\text{pTHz}^{1/2}$ range at 600 KHz. We stress that the bandwidth in our design is only subject to fluctuations of the biasing flux, since quantum error correction can correct for noise at all frequencies.

Comparing the energy scales of our system to the typical time scales of interferometry-based sensing schemes with trapped ions, we see that the ratio between the Hamiltonian strengths $\sim |dg_s/d\Phi_{\text{signal}}|A_{\text{coupler}}/\mu_B$ compensates for the fact that the ions hyperfine levels have longer lifetimes than *Xmon* circuits [34,44], by a factor of $\sim 10^5$, and places our design as a candidate for the determination of frequency standards. Nitrogen vacancy centers in diamond are another promising platform for sensing, with sensitivities in the $\text{nTHz}^{1/2}$ range and high spatial resolution [45–47]. Because of the lack of a tunable many-body signal term, it is currently unclear how to supplement this architecture with quantum error correction.

Considerations on pure dephasing.—We have identified two sources of dephasing noise against which our four-qubit code is ineffective. The logical information is therefore vulnerable to these errors and must be protected using other methods.

First, one approximation we have taken is that τ_{EC} can be arbitrarily short, increasing therewith sensitivity arbitrarily far beyond the relaxation limit. A consequence of τ_{EC} being finite, however, is an uncorrectable dephasing caused by uncertainty about when exactly decay happened between two consecutive rounds of correction. In the time lapse between a decay and its correction, the probe evolves outside the logical subspace. As a result, averaging over many realizations of the experiment effectively randomizes the accumulated signal. This problem is general in QEC-assisted metrology, yielding a decay rate of $(g_s\tau_{\text{EC}}/\hbar)^2\gamma$ [22], which can be mitigated by performing corrections extremely fast.

Second, for sensing alternating current magnetic fields $B = |B|\cos(\omega_B t)$, applying decoupling pulses at the

frequency of the alternating signal will refocus noise due to a fluctuating bias with correlation times longer than ω_B^{-1} . This is especially effective against low-frequency noise, and can indeed be used to push T_2 times to the relaxation limit. Importantly, given that these gates can be done very fast, this implies achievable bandwidths of up to several hundred MHz.

Summary and outlook.—We suggested a superconducting circuit design to measure magnetic fields with a precision that is not relaxation limited, by incorporating error correction into the sensing protocol. Correcting at a sufficiently high rate and gate fidelity can increase the lifetime by several orders of magnitude, and it seems possible to probe beyond the femto Tesla regime in the future. For the gate speeds and fidelities demonstrated in Refs. [35,36], we estimate each round of error correction to be achieved in $\sim 2 \mu\text{s}$. Current *Xmon* lifetimes are in excess of $40 \mu\text{s}$, meaning that the needed frequencies for error correction are achievable (see Fig. 3). Therefore, the only remaining impediment are gate fidelities, which should increase by an order of magnitude in order to observe an enhancement. This opens up the possibility to perform quantum metrology in a fault-tolerant manner, that is, probing signals at the logical level while fighting general quantum noise induced by the environment as well as by the correction procedure.

The authors acknowledge discussions with Martin Plenio, Pedram Roushan, and Michael Geller. D. A. H.-M. acknowledges partial support from a Hebrew University Fellowship, A. R. acknowledges support of the Israel Science Foundation (Grant No. 039-8823), the European Commission (Grant No. 323714), DIADEMS Project and the European CIG Grant No. 321798. D. A. acknowledges support from ERC Grant No. 030-8301.

-
- [1] W. H. Itano, J. C. Bergquist, J. J. Bollinger, J. M. Gilligan, D. J. Heinzen, F. L. Moore, M. G. Raizen, and D. J. Wineland, *Phys. Rev. A* **47**, 3554 (1993).
 - [2] S. F. Huelga, C. Macchiavello, T. Pellizzari, A. K. Ekert, M. B. Plenio, and J. I. Cirac, *Phys. Rev. Lett.* **79**, 3865 (1997).
 - [3] E. L. Hahn, *Phys. Rev.* **80**, 580 (1950).
 - [4] L. Viola and S. Lloyd, *Phys. Rev. A* **58**, 2733 (1998).
 - [5] L. Viola, E. Knill, and S. Lloyd, *Phys. Rev. Lett.* **82**, 2417 (1999).
 - [6] J. Bylander, S. Gustavsson, F. Yan, F. Yoshihara, K. Harrabi, G. Fitch, D. G. Cory, Y. Nakamura, J.-S. Tsai, and W. D. Oliver, *Nat. Phys.* **7**, 565 (2011).
 - [7] P. Facchi, D. A. Lidar, and S. Pascazio, *Phys. Rev. A* **69**, 032314 (2004).
 - [8] F. F. Fanchini, J. E. M. Hornos, and R. d. J. Napolitano, *Phys. Rev. A* **75**, 022329 (2007).
 - [9] P. Rabl, P. Cappellaro, M. V. Gurudev Dutt, L. Jiang, J. R. Maze, and M. D. Lukin, *Phys. Rev. B* **79**, 041302 (2009).

- [10] P. Chen, *Phys. Rev. A* **73**, 022343 (2006).
- [11] G. Gordon, N. Erez, and G. Kurizki, *J. Phys. B* **40**, S75 (2007).
- [12] J.-M. Cai, B. Naydenov, R. Pfeiffer, L. P. McGuinness, K. D. Jahnke, F. Jelezko, M. B. Plenio, and A. Retzker, *New J. Phys.* **14**, 113023 (2012).
- [13] P. W. Shor, *Phys. Rev. A* **52**, R2493 (1995).
- [14] A. Steane, *Proc. R. Soc. A* **452**, 2551 (1996).
- [15] R. Laflamme, C. Miquel, J. P. Paz, and W. H. Zurek, *Phys. Rev. Lett.* **77**, 198 (1996).
- [16] D. Gottesman, *Phys. Rev. A* **54**, 1862 (1996).
- [17] E. Knill *et al.*, Tec. Report No. LAUR-96-2199 LANL.
- [18] D. Aharonov and M. Ben-Or, in *Proceedings ACM Symp. Th. of Comp.* (ACM, New York, 1997), p. 176, ISBN 0-89791-888-6.
- [19] A. Y. Kitaev, *Ann. Phys. (Amsterdam)* **303**, 2 (2003).
- [20] R. Ozeri, [arXiv:1310.3432](https://arxiv.org/abs/1310.3432).
- [21] W. Dür, M. Skotiniotis, F. Fröwis, and B. Kraus, *Phys. Rev. Lett.* **112**, 080801 (2014).
- [22] G. Arrad, Y. Vinkler, D. Aharonov, and A. Retzker, *Phys. Rev. Lett.* **112**, 150801 (2014).
- [23] E. M. Kessler, I. Lovchinsky, A. O. Sushkov, and M. D. Lukin, *Phys. Rev. Lett.* **112**, 150802 (2014).
- [24] D. W. Leung, M. A. Nielsen, I. L. Chuang, and Y. Yamamoto, *Phys. Rev. A* **56**, 2567 (1997).
- [25] J. Koch, T. M. Yu, J. Gambetta, A. A. Houck, D. I. Schuster, J. Majer, A. Blais, M. H. Devoret, S. M. Girvin, and R. J. Schoelkopf, *Phys. Rev. A* **76**, 042319 (2007).
- [26] J. A. Schreier *et al.*, *Phys. Rev. B* **77**, 180502 (2008).
- [27] A. Houck *et al.*, *Phys. Rev. Lett.* **101**, 080502 (2008).
- [28] J. Koch, V. Manucharyan, M. H. Devoret, and L. I. Glazman, *Phys. Rev. Lett.* **103**, 217004 (2009).
- [29] N. A. Masluk, I. M. Pop, A. Kamal, Z. K. Mineev, and M. H. Devoret, *Phys. Rev. Lett.* **109**, 137002 (2012).
- [30] C. Rigetti *et al.*, *Phys. Rev. B* **86**, 100506 (2012).
- [31] D. A. Herrera-Martí, A. Nazir, and S. D. Barrett, *Phys. Rev. B* **88**, 094512 (2013).
- [32] M. R. Geller, E. Donate, Y. Chen, M. T. Fang, N. Leung, C. Neill, P. Roushan, and J. M. Martinis, *Phys. Rev. A* **92**, 012320 (2015).
- [33] R. A. Pinto, A. N. Korotkov, M. R. Geller, V. S. Shumeiko, and J. M. Martinis, *Phys. Rev. B* **82**, 104522 (2010).
- [34] R. Barends *et al.*, *Phys. Rev. Lett.* **111**, 080502 (2013).
- [35] R. Barends *et al.*, *Nature (London)* **508**, 500 (2014).
- [36] R. Barends *et al.*, *Nat. Commun.* **6**, 7654 (2015).
- [37] Y. Chen *et al.*, *Phys. Rev. Lett.* **113**, 220502 (2014).
- [38] B. Peropadre, D. Zueco, F. Wulschner, F. Deppe, A. Marx, R. Gross, and J. J. García-Ripoll, *Phys. Rev. B* **87**, 134504 (2013).
- [39] See Supplemental Material at <http://link.aps.org/supplemental/10.1103/PhysRevLett.115.200501> for a detailed description of the magnetometer design, a review of approximate quantum error correction and a sensitivity analysis.
- [40] E. Jeffrey *et al.*, *Phys. Rev. Lett.* **112**, 190504 (2014).
- [41] D. Vasyukov *et al.*, *Nat. Nanotechnol.* **8**, 639 (2013).
- [42] H. Xia, A. Ben-Amar Baranga, D. Hoffman, and M. V. Romalis, *Appl. Phys. Lett.* **89**, 211104 (2006).
- [43] M. Hatridge, R. Vijay, D. H. Slichter, J. Clarke, and I. Siddiqi, *Phys. Rev. B* **83**, 134501 (2011).
- [44] S. Kotler, N. Akerman, Y. Glickman, A. Keselman, and R. Ozeri, *Nature (London)* **473**, 61 (2011).
- [45] L. M. Pham, N. Bar-Gill, C. Belthangady, D. Le Sage, P. Cappellaro, M. D. Lukin, A. Yacoby, and R. L. Walsworth, *Phys. Rev. B* **86**, 045214 (2012).
- [46] J. R. Maze *et al.*, *Nature (London)* **455**, 644 (2008).
- [47] G. Balasubramanian *et al.*, *Nature (London)* **455**, 648 (2008).